frontiers | Frontiers in Astronomy and Space Sciences

TYPE Original Research
PUBLISHED 13 September 2023
DOI 10.3389/fspas.2023.1162624

OPEN ACCESS

EDITED BY
Jay R. Johnson,
Andrews University, United States

REVIEWED BY
Scott Alan Thaller,
Atmospheric and Space Technology Research Associates, United States
Ciarán D. Beggan,
Natural Environment Research Council (NERC), United Kingdom

*CORRESPONDENCE
T. M. Esman,
teresa.esman@nasa.gov

RECEIVED 09 February 2023
ACCEPTED 31 August 2023
PUBLISHED 13 September 2023

CITATION
Esman TM, Espley JR, Gruesbeck JR, Verbiscer A, Giacalone J and Halford AJ (2023), Will we find Martian lightning via Schumann resonances?
Front. Astron. Space Sci. 10:1162624.
doi: 10.3389/fspas.2023.1162624

Will we find Martian lightning via Schumann resonances?

T. M. Esman[1]*, J. R. Espley[2], J. R. Gruesbeck[2], A. Verbiscer[3], J. Giacalone[4] and A. J. Halford[2]

[1]NASA Postdoctoral Program Fellow, NASA Goddard Space Flight Center, Greenbelt, MD, United States, [2]NASA Goddard Space Flight Center, Greenbelt, MD, United States, [3]Department of Astronomy, University of Virginia, Charlottesville, VA, United States, [4]Planetary Sciences, Lunar and Planetary Laboratory, University of Arizona, Tucson, AZ, United States

Schumann resonances are electromagnetic resonances generally associated with lightning. If they exist on Mars, Schumann resonances are expected to resonate within the ionospheric cavity at a fundamental frequency of 7–14 Hz. We conducted a search for 5–16 Hz signals below 400 km in magnetic field data from the Mars Global Surveyor (MGS) and Mars Atmosphere and Volatile Evolution (MAVEN) missions. Fast Fourier transforms and wavelet analysis were used to find these signals and investigate their characteristics further. We discuss our null results and the required steps forward to continue and improve this search. Future studies will require higher sensitivity instruments and would benefit from additional missions that reach into the lower ionosphere of Mars.

KEYWORDS

Mars, Schumann resonance, magnetometer, ionosphere, lightning, waves

1 Introduction

With an idealized electrically conducting surface and a conducting ionosphere, a planet forms a global waveguide and traps low frequency electromagnetic energy. Terrestrial lightning discharges, with spatial scales on the order of kilometers, create broadband electromagnetic energy that resonates in this spherical shell cavity. These resonances are called Schumann resonances (SR) (Schumann, 1952). On Earth, they exhibit distinct peaks at extremely low frequencies (ELF) with fundamental frequencies around 8 Hz and observable harmonics up to at least 44 Hz. These signals are routinely used for the remote sensing of lightning. The SR fundamental frequency is in part determined by the radius of the planet, the distance between the planet surface and ionospheric peak, and the conductivity of both (Greifinger and Greifinger, 1976; Beamish and Tzanis, 1986; Sentman and Fraser, 1991; Grimm, 2002; Nickolaenko and Hayakawa, 2002). We note that mechanisms other than lightning have been presented as potential sources of Schumann resonances (Beghin, 2014).

Both experimental (Eden and Vonnegut, 1973; Krauss et al., 2006; Aplin et al., 2011) and theoretical work (Melnik and Parrot, 1998; Farrell et al., 1999; Renno et al., 2003; Zhai et al., 2006; Izvekova et al., 2022) suggest that charge separation sufficient for electrical discharges plausibly occurs in Martian atmospheric dust activity (e.g., global storms, regional storms, and local dust devils). Both terrestrial and martian instruments have detected changes in the magnetic field associated with dust devils approaching and receding from them (e.g., Houser et al., 2003; Charalambous et al., 2021). Whether electrical discharges would be primarily large scale, filamentary discharges similar to terrestrial thunderstorms, or primarily microscopic scale, intergrain glow discharges is unknown (Farrell and Desch, 2001). Both types of discharges potentially create broadband electromagnetic energy, but

only the large scale discharges likely produce appreciable energy at ELF frequencies (Farrell et al., 2000) sufficient to contribute to SR at Mars.

Regardless of the exact type of discharges that occur at Mars, the existence and investigation of any such events would be important for several reasons. Along with the intrinsic interest in a new discovery, these electromagnetic discharges could cause alterations in the chemistry at the surface and in the atmosphere. Lightning is the largest natural producer of nitrogen oxides in Earth's upper troposphere. Though it remains difficult to determine, the annual global mass of nitrogen produced via lightning-induced nitrogen oxides is estimated at 5 ± 3 Tga^{-1}(Schumann and Huntrieser, 2007, & references therein). Lightning has also been proposed as a possible explanation for the anomalous abundance of nitric oxides at Venus (Krasnopolsky, 2006). The existence of Venusian lightning has yet to be confirmed, though both radio and optical observations have been interpreted as lightning (Ksanfomaliti, 1980; Russell, 1991; Russell et al., 1993; Russell et al., 2006; Hansell et al., 1995).

Lightning poses a threat to future missions as electrical discharges are potentially hazardous to instruments, rovers, and astronauts (Hauck, 2002). Additionally, understanding the electromagnetic activity in the atmosphere introduces the possibility of using such energy to probe for subsurface cavities and conductivity (Grimm, 2002). Future missions which carry an instrument capable of measuring electric or magnetic fields would benefit from information regarding necessary sensitivities, expected signal amplitudes, and a better understanding of atmospheric and magnetic connections.

Several groups have created models to predict the characteristics of SR at Mars using both analytical and numerical modeling techniques (Sukhorukov, 1991; Pechony and Price, 2004; Molina-Cuberos et al., 2006; Yang et al., 2006; Soriano et al., 2007; Simoes et al., 2008b; Simoes et al., 2008a; Toledo-Redondo et al., 2017). These models use a variety of parameterizations for the surface conductivities, but in all cases (disregarding the unrealistic case of perfect conductivity) the fundamental frequency is predicted to be ~7–14 Hz. An important aspect not included in the models is the contributions from the crustal magnetic fields (CMFs), which are localized magnetization of crust, primarily in the southern hemisphere (Acuña et al., 1998). The CMFs create large local variations in the ionospheric densities (Nielsen et al., 2007), including transient ionospheric layers (e.g., Gurnett et al., 2005; Kopf et al., 2008; Kopf et al., 2017; Kim et al., 2012; Matta et al., 2015; Zhang et al., 2015; Mayyasi et al., 2018). The CMF-driven fluctuations in the structure of the ionosphere alter the resonant cavity, potentially resulting in global changes to the expected range of frequencies.

Observing signals from atmospheric electricity at Mars has been a goal for many. Ruf et al. (2009) used a receiver piggy-backing on the Deep Space Network to observe Mars at about 8.5 GHz and, by using the kurtosis of that signal, found significant energy at about 10, 28, and 32 Hz. These observations were interpreted as being produced by a strong regional dust storm at Mars occurring at the time of the observation. However, the electric field associated with the implied SR would have to be approximately a thousand times greater than the electric field in terrestrial thunderstorms (Ruf et al., 2009). We note that incredibly powerful lightning or "superbolts" have been observed at Earth (e.g., Turman, 1977; Holzworth et al., 2019). If the signal observed by Ruf et al. (2009) was powerful lightning, Schumann resonances should be observable by present-day magnetometers at Mars (further discussed in Section 5).

Subsequent observations of Mars taken with the Allen Telescope Array during a time *lacking* dust storms showed no signs of significant energy at the expected frequencies of SR as the only signals present were caused by terrestrial radio frequency interferences (Anderson et al., 2012). Attempts to observe the broadband energy at radio frequencies of approximately 5 MHz by the Mars Advanced Radar for Subsurface and Ionosphere Sounding (MARSIS) onboard Mars-orbiter Mars Express also showed no significant power (Gurnett et al., 2010). Similarly, there have been no successful attempts at direct optical imaging of electrical discharges at Mars (e.g., Farrell et al., 2000).

The Martian ionosphere is a region of charged particles, or plasma, in the upper atmosphere and lower region of the magnetosphere (Russell, 1995). Though both are highly variable, the upper limit of the Martian ionosphere occurs at 400–500 km (Mitchell, 2001; Mitchell, 2001; Brain et al., 2006; Brain et al., 2006; Duru, 2009; Duru, 2020; Duru, 2009; Duru, 2020) and the ionospheric density peaks around 140 km (e.g., Hanson et al., 1977; Withers et al., 2012; Vogt et al., 2016). The solar wind is the upper boundary of the ionosphere and influences the plasma and magnetic environments. Changes in space weather as well as inter-annual and seasonal changes can produce variations in the ionosphere, including the altitude of the ionospheric peak (Withers et al., 2006).

Because of this known variability, the upper boundary of the cavity is far from a simple, idealized obstacle and our search is not strictly limited to 7–14 Hz. Though extremely rare, there have also been observations of terrestrial SR leaking beyond the ionospheric peak (Simoes et al., 2011), albeit signals that were considerably lower in strength than those observed within the ionospheric cavity. Greifinger and Greifinger (1976) showed that the energy in such a wave (and therefore amplitude) is fairly constant for terrestrial altitudes above 100 km. Based on the limited terrestrial observations of SR beyond the ionospheric peak and the reduction of wave power, observing SR at Mars above the ionospheric peak is very unlikely. Regardless, the possibility still exists as the Martian ionosphere and magnetic environment are very different from the terrestrial equivalents. Of particular interest, the nightside Martian ionosphere exhibits patchiness and irregularities (Safaeinili et al., 2007; Gurnett et al., 2008; Lillis et al., 2009; Němec et al., 2010; Němec et al., 2011; Withers et al., 2012) that could facilitate leaking. All these factors considered, our Martian search is altitude-limited to below 400 km and frequency-limited to 5–16 Hz.

We analyze data from the Mars Global Surveyor (MGS) (Albee et al., 2001) and the Mars Atmosphere and Volatile Evolution (MAVEN) (Jakosky et al., 2015) mission magnetometers for magnetic signals above 5 Hz at altitudes below 400 km. We briefly discuss the null results and difficulties with the magnetometer on the Interior Exploration using Seismic Investigations, Geodesy and Heat Transport (InSight) mission (Banerdt and Russell, 2017). In Section 2, we discuss the datasets used. In Section 3, we discuss methods used to isolate signals of interest. In Section 4, we discuss the results of the searches. We explore detectability limitations in Section 5. Finally, Section 6 contains the concluding remarks and comments on the future of searches for Martian SR.

2 Data

MAVEN began orbiting Mars in September 2014 and remains active (as of 2023). The MAVEN magnetometer (MAG) consists of dual fluxgate magnetometers that provide magnetic field vector data at a 32 Hz sampling rate Connerney et al. (2015). The MAVEN MAG dataset (PDS, 2022) used in this study contains data from Sept. 2014 through Feb. 2019, which includes data from the northern autumn of Mars year (MY) 32 to Northern winter of MY 34. Seasonal variability is influential to the climate and dust activity as the orbit of Mars is relatively elliptical. This time period includes one regional dust storm (MY 32), a local dust storm (MY 33), and the 2018 planet encircling dust event of MY 34 (e.g., Withers et al., 2018; Girazian et al., 2019; Guzewich et al., 2019; Montabone et al., 2020). These events, especially the MY 32 event, provide a critical opportunity to search for signals during conditions more similar to Ruf et al. (2009) conditions. The MY 29 (2009) dust storm was regional and highly variable, but similar to the MY 32 event in optical depth change and season (near L_s = 230).

MAVEN MAG data below 400 km were examined, which totaled more than 2,600 h of data from over 8,600 orbits and included 9 Deep Dip campaigns. The Deep Dip campaigns were special orbits with periapses reduced down to around 130 km. There are known MAVEN-generated signals (Connerney et al., 2015). These include 0.1–10 Hz reaction wheel-related signals of ~0.1 nT and ~0.5 nT near-instantaneous discontinuities caused by solar array switching. Thruster firings, which are planned events, can cause ~5 nT oscillations.

The MGS spacecraft was active at Mars from September 1997 until November 2006. The MGS MAG consisted of dual triaxial fluxgate magnetometers included in the science payload, with sensors at the end of each solar array panel (Acuña et al., 2001). Non-environmental signals from spacecraft components, notably the high gain antenna and the power subsystem and/or circuits on the solar array panels were detectable by MAG. However, these are known, well-characterized signals.

There were two phases to the MGS mission; the pre-mapping phase and the mapping phase (Albee et al., 2001). During the mapping phase, MGS circled in a polar orbit in order to collect global images and data. In the time before this phase, the MGS orbit was more eccentric and reached altitudes below the ionopause (Cloutier et al., 1999). For this reason, our focus is on the pre-mapping phase (1997–1999). Again, we focused on data from altitudes less than 400 km (PDS, 2007). It is important to note that the altitude of the spacecraft, and therefore the measurements, was determined by subtracting the volumetric radius (3,389.5 km) of Mars from the location of the spacecraft in sun-state coordinates (i.e., a coordinate system which has an origin at the center of the planet). This means that the altitude is a proxy for the distance to the ground, but the actual distance varies with topology [i.e., Olympus Mons (~22 km) would be the largest discrepancy]. This is adequate for our investigation as our search was already expanded to include higher altitudes.

Once filtered to altitudes below 400 km, the MGS data are severely limited compared to the full MGS MAG dataset. For example, there are no remaining data available from the nightside. The majority of the data in the intervals were taken during the northern Martian autumn (solar longitude, 180° < L_s < 270°) and none were taken in the Northern Martian summer (90° < L_s < 180°). This is important to note as Martian dust activity is known to vary with season (Heavens et al., 2014), but during this time period there were no global dust events (e.g., Shirley, 2015).

MGS MAG data are available in two coordinate systems; payload and sun-state, which is the same as Mars-centered Solar Orbital (MSO). MSO is a coordinate system in which + X points along the Mars-Sun line, +Y is antiparallel to Mars' orbital velocity, and +Z completes the right-handed coordinate system. The payload coordinate system is the frame of reference of the spacecraft, where + Z is upwards from the spacecraft and follows the direction of spacecraft motion through the Martian atmosphere during aerobraking (cf. Albee et al. (2001); Figure 4). Data in payload coordinates more clearly exhibit spacecraft interference and contamination of the data, which can then be excluded from the study. As the spacecraft rotates through space (as MGS did during its pre-mapping phases at about one rotation every 2 hours), if a signal persists in a fixed direction in spacecraft payload coordinates, it most likely originates from the spacecraft itself; an environmental signal would not be expected to rotate with the spacecraft. The data are labeled in the format "m##d###", where the numbers following 'm' are the year and the numbers following the "d" are the day of year.

With both MGS and MAVEN datasets, the overall coverage for the Schumann resonance search was 1997–1998 and 2014–2019.

InSight landed on Mars in November 2018 in Elysium Planitia. The InSight Fluxgate Magnetometer (IFG) was part of the Auxiliary Payload Sensor Subsystem (APSS) (Banfield et al., 2018), which is a suite of environmental-monitoring instruments. The IFG was not a primary science instrument. Regardless, as the lander provided the first ever ground-based Martian magnetometer data, we performed a cursory search of the high time resolution (20 samples/second) IFG data (Russell and Joy, 2021) for signals of 5–10 Hz. The high time resolution data was limited to specific time intervals due to downlink bandwidth constraints.

3 A semi-automated method for wave searches

A multi-step process to identify periods of possible wave signals in MAVEN MAG data was developed. The method is similarly described in Esman et al. (2021), Esman et al. (2022), and Esman (2022).

Fast Fourier transforms (FFTs) of each component of the magnetic field time series were used to create a comparative and quantitative guide for a visual search of waves. Each 10 s FFT overlapped the previous FFT by one second to ensure signals would not be lost at the edges of FFTs.

The power from the FFTs was averaged over 5–16 Hz and summed across the components to remove coordinate system dependence. FFTs were only calculated for continuous data intervals. The result is a time series of magnetic fluctuation power for the entire input dataset, which indicates periods of possible wave activity with enhanced spectral power when compared to the average spectral power. In other words, if waves are present, there is an enhancement in the FFT at the wave frequency, which translates to an enhancement in power. Because of the digital resolution of

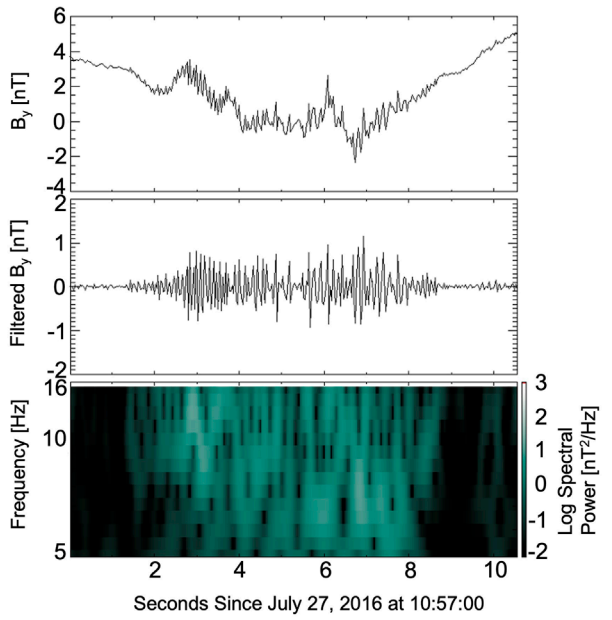

FIGURE 1
A signal found in the MAVEN data is shown with power in a range of frequencies. The Y-direction magnetic field and the Y-direction magnetic field filtered to 5–16 Hz are shown in the first two panels, respectively. The other magnetic field directions are excluded for space and clarity. The final panel is the wavelet of the unfiltered Y-direction magnetic field, which shows that the signal exhibits power in the full range of interest (5–16 Hz).

the magnetometers, we place a lower limit of 0.01 nT on wave amplitudes.

The methods described above are used with the primary purpose of identifying potential wave signals in magnetic field data. Further analysis is conducted for each of these identified signals. This begins with wavelet analysis. Wavelet transforms provide time and frequency information through power spectra. Morlet wavelets (Torrence and Compo, 1998), which are sine waves tapered by a Gaussian, are used for the analysis of the dataset. Recalculated FFTs for the duration of the wave (not restricted to 10 s) provided specific primary (i.e., most powerful) wave frequencies. Broadband or temporally overlapping events can result in power signatures over a broad range of frequencies (e.g., see Figure 1). This means that waves with primary frequencies outside the range of interest can be identified with this method. MAVEN results are found in Section 4.1. MGS results are found in Sections 4.2,4.3.

3.1 Starting with a "by eye" search for MGS

MGS MAG data were initially investigated by eye. This method is, of course, biased based on the individual determining which signals are or are not waves. Wavelet and FFT analysis was conducted on the waves. The FFTs were used as a check for any significant spectral peaks. The data were examined in both MSO and payload coordinates. The multi-coordinate system analysis is necessary for MGS to better determine which signals are spacecraft-generated signals. This is not necessary for MAVEN, because the suite of instruments provide sufficient information for identifying spacecraft-generated signals.

The "by eye" study was followed by a completely separate reanalysis of the MGS data using the semi-automated method developed for the MAVEN data. The potential SR signals found by the two MGS studies and a discussion of the effectiveness of both methods are in the next section. The MAVEN data were not searched purely by eye.

4 Schumann resonance search results

4.1 MAVEN results

A total of 86 signals of interest were found within the MAVEN data below 400 km. None of the identified signals matched signals known to originate from the MAVEN spacecraft itself (Connerney et al., 2015). However, we also determined that none of these were SR. Wavelets revealed that some waves were at primary frequencies much lower than 7 Hz. The average frequency of the signals was 6.58 Hz with a standard deviation of 2.16 Hz. A unavoidable consequence of wavelet analysis is a reduction in temporal and frequency resolution, which can result in power from specific frequencies 'bleeding' into other frequencies, albeit with weaker power. Other potential signals exhibited strong power in a wide (e.g., the full 5–16 Hz range) range of frequencies indicating the signal was not produced by SR. Figure 1 shows an example of one of the potential SR signals and the associated broadband spectral power. Observations of terrestrial SR are seen to have full width half maximums of less than 5 Hz (e.g., Votis et al., 2018). Further, we eliminated signals that matched the MAVEN reaction wheel frequencies and times, which are available publicly (Harter, 2022). All signals were compared with the reaction wheel data. See Esman et al. (2022) for discussion of signals below 200 km and a more in depth follow-up investigation (e.g., the addition of other instrument data sets).

4.2 MGS "by eye" results

The visual search of the MGS MAG data resulted in no identified SR. Three days (m97d343 or 9 December 1997, m98d009 or 9 January 1998, and m98d094 or 4 April 1998) exhibited narrowband (i.e., a couple Hz width) signals at appropriate frequencies, but were all determined to be spacecraft-generated signals (e.g., reaction wheels, which had not previously been specifically identified in the MGS data). The strongest of the signals extended beyond 1 R_M into the magnetosphere, demonstrating the signal was from MGS. The other two signals maintained power in only one of the spacecraft coordinate axes, even as the spacecraft was aerobraking. Sections 4.2.1,4.2.2 discuss these three events in more detail.

4.2.1 Events limited to the ionosphere

Intervals from 2 days (m97d343 and m98d009) were especially promising as the signals were observed at altitudes below 150 km. The signal on m98d009 was approximately 3.6 min in length. In the payload coordinate frame, the signal is entirely

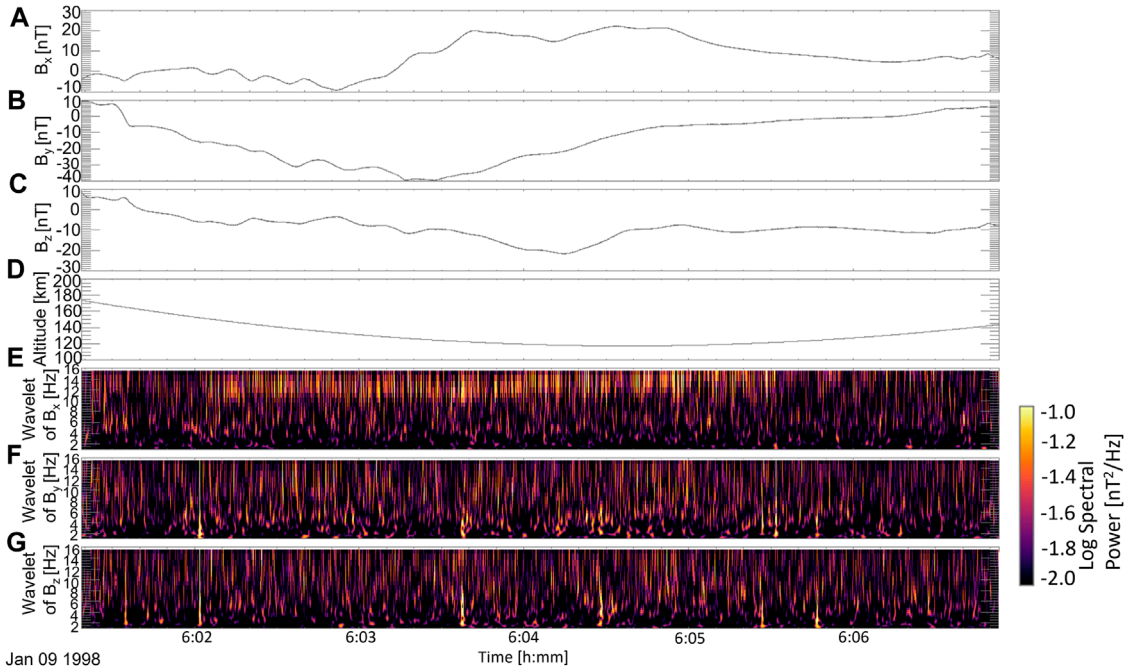

FIGURE 2
MGS MAG data, altitude, and wavelets for m98d009 (9 January 1998) in payload coordinates. The first three panels **(A–C)** are the magnetic field in the X, Y, and Z direction. The fourth panel **(D)** is altitude in km. These are followed by the corresponding X, Y, and Z direction wavelets **(E–G)**. A signal at around 12 Hz is visible in only the X-direction wavelet **(E)**, indicating this is a spacecraft-associated signal.

in the X-direction. Figure 2 shows the m98d009 signal in payload coordinates. Figures 2A–C show the magnetic field strength. The comparatively high frequency signals we are interested in are embedded in large scale variations (~10 nT). Figure 2D shows the altitude of the spacecraft at the time of measurement. The Figures 2E–G show the wavelet spectra. The signal is only visible in the X-direction wavelet (Figure 2E). After filtering the magnetic field data to frequencies between 1 and 16 Hz, we find that the peak-to-peak amplitude is about 0.2 nT.

The signal from m97d343 is also embedded in large scale, low frequency ionospheric variations, but is itself quite low in amplitude (~0.2 nT peak-to-peak) relative to the noise environment. It lasts about 34.5 s and is only seen in the Z-direction in the payload frame.

As previously stated, the likelihood of an environmentally produced signal being confined exclusively to one direction in the spacecraft frame is extremely low. Therefore, we conclude these two signals are spacecraft-generated. This is further validated given that MGS was usually moving (spinning or reorienting) during these aerobraking passes.

4.2.2 The magnetosphere-reaching event

A single MGS event presented a particularly prominent, clear, narrow-band, and powerful signal below 400 km. The signal, from m98d094, is shown in payload coordinates in Figure 3. Spectral magnitude power is predominately in the payload X, though the same signal can be seen in Y. In X, the signal has a peak-to-peak of ~0.5 nT. This signal was the most promising candidate for a Schumann resonance. However, further investigation revealed that the signal extended, continuous, for over a thousand kilometers into the magnetosphere. Therefore, it is clear that this signal is not lightning-related and instead is of spacecraft origin. Based on the known amplitudes of reaction wheels from MAVEN MAG [often at least 0.1 nT peak-to-peak (Connerney et al., 2015)], this signal is consistent with expected MGS reaction wheel interference. We conclude that this signal is of spacecraft origin.

4.3 MGS reanalysis results

Using the methodology described in Section 3, the reanalysis of the MGS MAG data resulted in seven additional wave signals. This analysis was completely separate to the "by eye" search discussed in Section 4.2.

Four of the additional wave signals exhibited behaviors and frequencies inconsistent with SR, but warrant future analysis. There were three potential SR signals, which had not previously been found by eye. See Table 1 for a list of the potential signals and their detection method. Of these three, two (m97d347 or 13 December 1997 and m99d058 or Feb. 27, 1999) were coincidentally identified by eye after investigating a peak in spectral power that occurred 15 min and 30 min later, respectively. The 97d347 signal started at around 700 km and continues, fluctuating in frequency from 1–16 Hz, down to around 200 km and is only visible in the X-direction payload. Therefore, the m97d347 signal is likely spacecraft-generated.

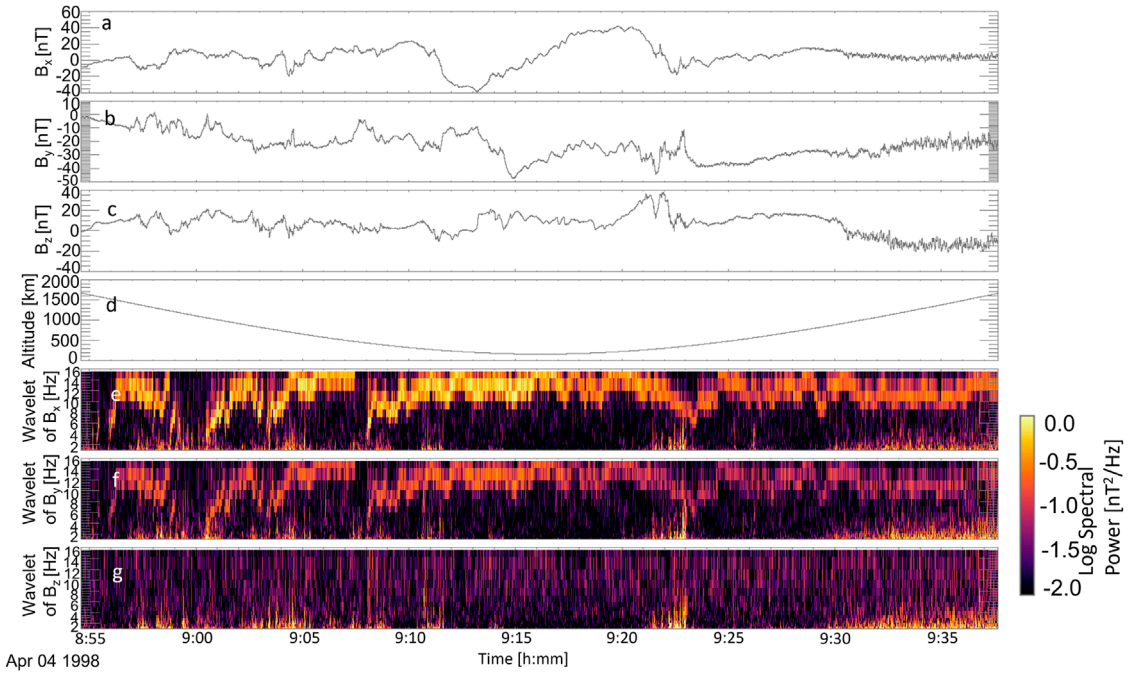

FIGURE 3
MGS MAG data, altitude, and wavelets from m98d094 (4 April 1998) in payload coordinates. The first three panels **(A–C)** are the magnetic field in the X, Y, and Z direction. The fourth panel **(D)** is altitude in km. These are followed by the corresponding X, Y, and Z direction wavelets **(E–G)**. The X-direction **(E)** wavelet shows the strongest feature found in the dataset within our search criteria. The signal stays prominent in the X-direction and extends beyond the bow shock. The signal is spacecraft interference.

TABLE 1 Potential SR Events Identified in the MGS dataset.

Day	Approximate start time (hh:mm)	Found by eye	Found with semi-auto method	Comments
m97d340	02:18	No	Yes	
m97d343	21:32	Yes	Yes	
m97d347	15:01	Yes	No	nearby spectral power peak
m98d009	06:02	Yes	No	Weak signal
m98d094	08:55	Yes	Yes	
m99d058	04:40	Yes	No	Found while looking at nearby spectral power peak

The m99d058 signal, seen in Figure 4, was perhaps the most promising signal found during the reanalysis. Just barely above 400 km, the signal is seen prominently in the payload Y-direction wavelet and very weakly in the X-direction wavelet. The amplitude of the oscillations are consistent (~0.2 nT peak-to-peak) with reaction wheels and the power never fluctuates between magnetic field components. This is also likely a spacecraft-generated signal.

The signal from m97d340 is a narrow-band signal that meets our initial criteria, yet was not identified by eye. Figure 5 shows, similarly to previous figures, that the wave is only present in one payload direction and is a spacecraft-generated signal.

The semi-automated method was able to find two of the previously identified signals (see Section 4.2). The third, m98d009 (Figure 2), was too weak to be found by the semi-automated method. It is evident that the semi-automated method misses weaker waves, which could be found with "by eye" analysis. Regardless, the time series of spectral power still guided the search, resulting in additional identified signals. Though clearly beneficial for finding signals, the "by eye" analysis is biased by the data analyst's judgement. The semi-automated method missed half of the total identified MGS signals, therefore we estimate another 86 signals could have been found via "by eye" analysis of the MAVEN data. This addition would certainly increase the statistical significance of the results. Developing a more robust method for wave searches, while maintaining lower false positives and finding as many signals as possible, is a priority for the future.

4.4 InSight results

As the IFG was not a primary science instrument and was a magnetometer with limited distance from other instruments on InSight, noise was expected in the data. An initial cursory search of the 20 Hz IFG data for 1 December 2018 was performed.

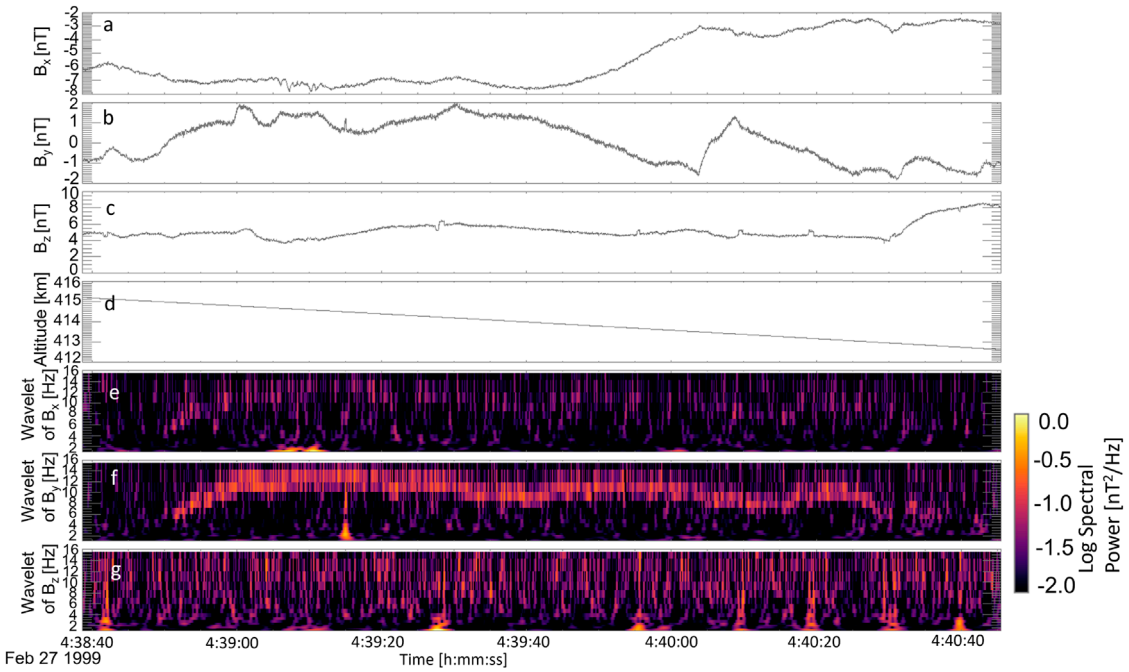

FIGURE 4
MGS MAG data, altitude, and wavelets from m99d058 (27 February 1999) in payload coordinates. The first three panels **(A–C)** are the magnetic field in the X, Y, and Z direction. The fourth panel **(D)** is altitude in km. These are followed by the corresponding X, Y, and Z direction wavelets **(E–G)**. The Y-direction wavelet **(F)** shows the strongest power of the signal, but it is also echoed in the X-direction wavelet **(E)**. The signal is likely spacecraft-generated as the power level stays consistent across the X- and Y-directions and the amplitude of the oscillations is consistent with reaction wheels. This is an example of a signal found by eye, while using the semi-automated technique.

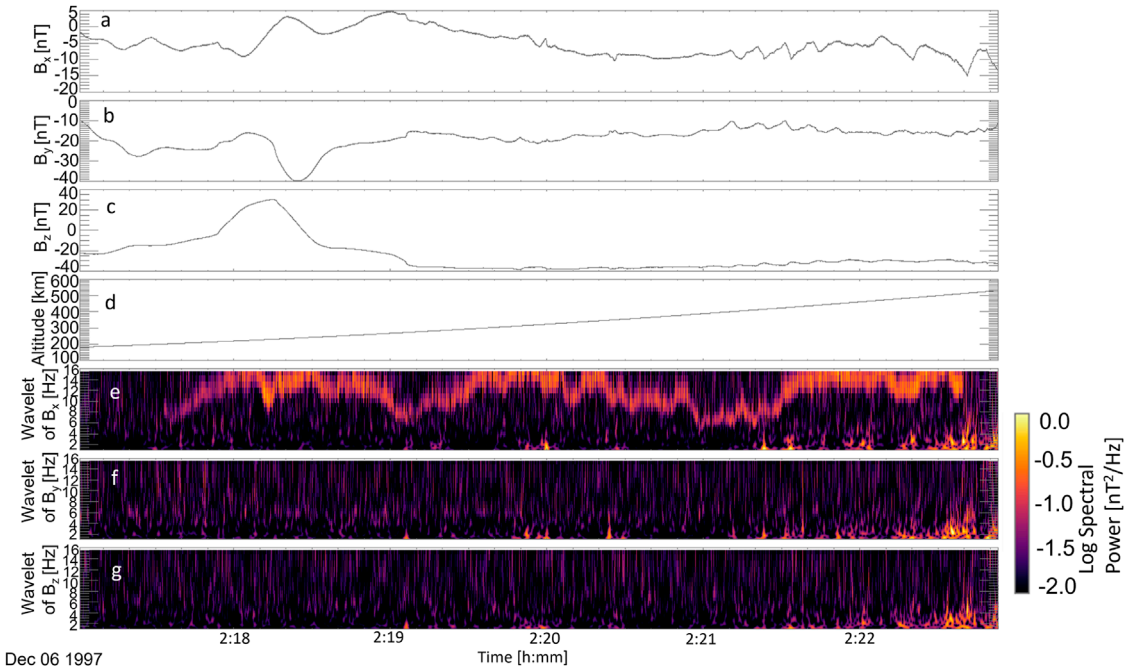

FIGURE 5
MGS MAG data, altitude, and wavelets from m97d340 (6 December 1997) in payload coordinates. The first three panels **(A–C)** are the magnetic field in the X, Y, and Z direction. The fourth panel **(D)** is altitude in km. These are followed by the corresponding X, Y, and Z direction wavelets **(E–G)**. The X-direction wavelet **(E)** shows a strong feature. The signal is likely spacecraft-generated as it stays prominent in the X-direction only and extends up to around 600 km. This is an example of a signal found using the semi-automated method, yet missed by the initial visual inspection.

Unsurprisingly, the data artifacts were too significant in the frequencies of interest and it was impractical to search for SR in the IFG data. Multiple identified data artifacts are described in Joy and Rowe (2019), including artifacts found in the low time resolution data and/or the high time resolution data. The report also indicates it is unlikely the artifacts will be removed from the high time resolution data. Future missions may provide better ground- or helicopter-based magnetometers on Mars.

5 An exploration of detectability limits

Terrestrial SR detected at ground level have signal strengths on the order of 0.001–0.01 nT (Füllekrug, 1995), so such signals were not expected to be detected. However, if, as suggested by Ruf et al. (2009), the electric fields producing the Martian Schumann signals are a thousand times the electric fields in the terrestrial Schumanns, then such signals should easily be discernible in our dataset as the wave power is proportional to the amplitude squared.

To provide a more quantitative response to our finding, we follow the calculation done by Farrell et al. (1999) (Section 4; Eqs. 7-10); Table 1) to estimate the lower constraint on power and upper constraint on occurrence rate for SR on Mars. For a frequency (f) range of 5–16 Hz, α_{SR} = 31–100 s^{-1} ($f = \alpha/2\pi$). We continue with α_{SR} = 100 s^{-1}, as this leads to the highest possible SR amplitude. With α_{VLF} = 20,000 s^{-1}, Farrell et al. (1999) calculate $E_{VLF} \sim 60 Q_{ac} \frac{h}{r}$, where Q_{ac} is the charge transported by the discharge process, h is the height of the storm/dust devil, and r is the distance between the observer/spacecraft and the center of dust activity. Therefore, we find:

$$\mathbf{E_{SR} \sim \frac{60}{20,000^2} \times \alpha_{SR} Q_{ac} \frac{h}{r} = 0.0015\ Q_{ac} \frac{h}{r}}. \quad (1)$$

Choosing the most intense Martian dust devil parameters from Table 1 in Farrell et al. (1999) (h = 10 km, Q_{ac} = 2.5 C) and a distance to MAVEN of 200 km, a maximum E_{SR} = 0.00019 V/m. We then convert the radiated E field to a very simplified expected magnetic field amplitude (B).

$$\mathbf{E_{SR} = cB_{SR}}, \quad (2)$$

where c is the speed of light. This leads to:

$$\mathbf{B_{SR} = E_{SR}/c = 6.25 \times 10^{-13}\ T = 0.625\ pT}, \quad (3)$$

which is not observable by the fluxgate magnetometers at Mars. However, using the result from Ruf et al. (2009), E_{Ruf} = 1000E_{SR} and B_{Ruf} = 0.63 nT. Therefore, the MAVEN and MGS magnetometers would not be able to resolve the expected strongest SR from dust devils, but would be able to find Martian SR from lightning 1,000 times more powerful than expected Martian dust devil lightning. The following equations, Eqs (4), (5), show the resulting SR amplitude from SR 1000 times more powerful than terrestrial lightning would also be detectable. For this calculation, Q_{ac} = 3 as used in Farrell et al. (1999).

$$\mathbf{E_{\oplus} = 0.0015 \star 3 \star \frac{5}{200} = 0.00011\ V/m} \quad (4)$$

$$\mathbf{B_{\oplus} = 3.7 \times 10^{-13}\ T = 0.37\ pT} \quad (5)$$

Due to potential spacecraft magnetic noise and instrumental offset variations, signals observed by MAVEN which are smaller then 0.2 nT should be treated carefully. Nonetheless, MAVEN MAG's numerical resolution allows signals as small as 0.01 nT. Taking this as the absolute lower limit for detectability with MAVEN, we set B_{SR} = 0.01nT. Then, $E_{SR} = cB_{SR}$ = 0.003 V/m. From $E_{SR} \sim 0.0015\ Q_{ac} \frac{h}{r}$ (h = 10 km, r = 200 km), we find Q_{ac} = 40 C. So, for the MAVEN MAG to observe SR, the discharge must be at least 13.3 times the terrestrial thunderstorm Q_{ac} and 16 times the most intense Martian dust storm Q_{ac}.

MAVEN travels at around 5 km/s and we have been using r = 200 km. Only considering data at 200 km or lower for a more conservative estimate, there were no discharges of 40 C or greater within 200 km of MAVEN over 1,124 h. Assuming a non-overlapping square area projected onto the surface of Mars, this very roughly translates to 8×10^9 km^2 ground coverage over the 1,124 h.

Farrell et al. (1999) finds that the limiting charge density for the Martian atmosphere is about 200 e/cm^3. Unfortunately, for the overwhelming majority of time, the electron density at our lower limit altitude of ~120 km is already beyond 200 e/cm^3 [e.g. (Fowler et al., 2015)]. Depletions of electrons reaching higher altitudes (160 km) have been observed, with a greater likelihood of this occurring on the nightside [e.g. (Girazian et al., 2023)]. However, the exact occurrence rate and duration of these depletions is not known and the depletions would have to correspond with dust activity. This suggests that, similar to the occurrences at Earth, SR detection at higher altitudes may be extremely rare.

Our analysis of the MGS MAG, MAVEN MAG, and InSight IFG datasets resulted in no clear signs of electrical discharges in the Martian ionosphere. With our imposed lower limit of 0.01 nT, our study would have found SR 100 times more powerful than Earth lightning. Therefore, any signals weaker than that could exist at Mars. A weaker SR-related signal occurrence rate would still likely be limited by the atmospheric density and dust activity.

In the MGS data, the signals discovered within the expected range for SR on Mars were determined to be spacecraft-related. Interesting naturally-driven signals were found in the MAVEN data, but were determined to not be SR. The high time resolution IFG data proved too contaminated for any effective search for SR. We conclude that any atmospheric electricity present at Mars cannot produce SR that are multiple orders of magnitude greater in power than terrestrial ones. Additionally, the Ruf et al. (2009) signal likely has an origin unrelated to lightning. This search cannot preclude electric activity typical of terrestrial SR or atmospheric electricity (e.g., glow discharges) that are not expected to produce SR.

An understanding of the theoretical largest scale electrical discharge that could be plausibly generated within a global, regional, or small-scale event helps constrain sensitivity requirements. However, conclusions have been inconsistent. Experimental work by Harper et al. (2021) removed interactions between grains and surfaces inconsistent with the Martian environment (e.g., containment walls). They determined that small-scale discharges are plausible and that the maximum charge densities distribution on the particles is on the order of 10^{-6} C/m^2. They note these small-scale discharges are potentially similar to discharges within terrestrial volcanic vents. Theoretical work by Farrell et al. (1999) demonstrated that discharges were possible within dust clouds on Mars. Additional details about lightning throughout the Solar

System can be found in Yair (2012) and Riousset et al. (2020). A mission with the specific goal of looking for evidence of lightning may be required to bring the necessary technology to Mars.

6 Conclusion

In this study, we conducted a search for 5–16 Hz signals below 400 km in the Martian magnetic field to determine if any lightning-related Schumann resonances could be identified. No such signals were found in the magnetic field data from the Mars Global Surveyor (MGS) or Mars Atmosphere and Volatile Evolution (MAVEN) missions. Future missions require a sensitivity greater than 0.01 nT to detect terrestrial-strength SR on Mars. Ideally, the sensitivity would be significantly higher for the detection of smaller-scale electrical discharges and the signals that leak out of the ionospheric cavity. This high sensitivity requirement introduces economic and structural obstacles for spacecraft.

There are two primary methods for detecting SR: electric and magnetic field measurements. A variety of antennae and magnetometers have been used as sensors. To achieve the necessary sensitivity at the required frequencies, a low noise induction coil or search coil magnetometer with 10,000–100,000 turns of copper wire is suggested (Sentman, 1995). A portable induction coil magnetometer system capable of SR detection is presented in Votis et al. (2018). The weight of one of the developed magnetic field antennas is 2.2 kg, which is 10 times the weight of the Juno Waves search coil (Sentman, 1995; Kurth et al., 2017). The limitations that future missions searching for SR face are, therefore, primarily weight, cost, and reducing noise from the main spacecraft and other science instruments included in a payload. Further technological advances may be necessary to make this feasible.

Additional missions that reach low into the ionosphere of Mars would benefit this search and the overall understanding of the Martian plasma environment. Reaching lower altitudes is difficult for orbiting spacecraft, while landers, rovers, and helicopter/drone-like missions can have increased noise contamination due to multiple instruments being physically close. Again, technological advancements may aid in mitigating these issues. For example, a helicopter mission that could deploy a magnetometer on a long boom could increase the distance between the magnetometer and other instruments.

Terrestrial- and smaller-scale electrical discharges on Mars have yet to be ruled out or observed. Electric fields or non-Schumann resonance signals may be a better method for ultimately finding lightning on Mars. The safety of instruments and astronauts remain a concern, as electrical discharges at Mars on smaller scales plausibly exist within the dusty environment.

Data availability statement

Publicly available datasets were analyzed in this study. This data can be found here: Planetary Data System (pds.nasa.gov). Mars Global Surveyor magnetometer data is available at: https://pds-ppi.igpp.ucla.edu/search/?sc=Mars%20Global%20Surveyor&t=Mars&i=MAG. Mars Atmosphere and Volatile Evolution magnetometer data is available at: https://pds-ppi.igpp.ucla.edu/search/view/?id=pds://PPI/maven.mag.calibrated. InSight magnetometer data is available at: https://pds-ppi.igpp.ucla.edu/search/view/?f=yes&id=pds://PPI/insight-ifg-mars.

Author contributions

TE conducted the MGS analysis as part of her undergraduate thesis under the guidance of JE and AV. TE conducted the MAVEN and InSight analysis as part of her graduate dissertation under the guidance of JE, JRG, and JG. TE conducted the semi-automated analysis for MGS and the comparison with the previous MGS search as part of her postdoctoral work with AH. TE wrote the paper and JE, JRG, JG, AV, and AH were part of the science discussion and editing, while providing advice and suggested additions to the paper. All authors contributed to the article and approved the submitted version.

Funding

This study was supported by TE's NASA GSFC summer internship, the University of Virginia, NASA funding for the MAVEN project through the Mars Exploration Program, the University of Arizona (Grant: 80NSSC18K0881) and by TE's appointment to the NASA Postdoctoral Program at the GSFC, administered by Oak Ridge Associated Universities under contract with NASA. AH was funded by the Space Precipitation Impacts project through the Heliophysics Internal Science Funding Model at NASA GSFC.

Acknowledgments

We would like to thank the MAVEN team, the UVA Astronomy department, the heliophysics group at the University of Arizona, the NASA Postdoctoral Program, and the Space Precipitation Impacts team at NASA GSFC.

Conflict of interest

The authors declare that the research was conducted in the absence of any commercial or financial relationships that could be construed as a potential conflict of interest.

Publisher's note

References

Acuña, M., Connerney, J. E. P., Wasilewski, P., Lin, R. P., Anderson, K. A., Carlson, C. W., et al. (1998). Magnetic field and plasma observations at mars: initial results of the mars global surveyor mission. *Science* 279, 1676–1680. doi:10.1126/science.279.5357.1676

Acuña, M. H., Connerney, J. E., Wasilewski, P., Lin, R. P., Mitchell, D., and Anderson, K. A. (2001). Magnetic field of Mars: summary of results from the aerobraking and mapping orbits. *Journal of Geophysical Research: Planets* 106, 23403–23417.

Albee, A. L., Arvidson, R. E., Palluconi, F., and Thorpe, T. (2001). Overview of the mars global surveyor mission. *J. Geophys. Res.* 106, 23291–23316. doi:10.1029/2000je001306

Anderson, M. M., Siemion, A. P. V., Barott, W. C., Bower, G. C., Delory, G. T., de Pater, I., et al. (2012). The allen telescope array search for electrostatic discharges on mars. *Astrophyical J.* 744, 15. doi:10.1088/0004-637x/744/1/15

Aplin, K. L., Davis, C. J., Bradford, W. J., and Herpoldt, K. L. (2011). Measuring martian lightning. *J. Phys. Conf. Ser.* 301, 012007. doi:10.1088/1742-6596/301/1/012007

Banerdt, W. B., and Russell, C. T. (2017). Editorial on: topical collection on insight mission to Mars. *Space Science Review* 211. doi:10.1007/s11214-017-0414-0

Banfield, D., Rodriguez-Manfredi, J. A., Russell, C. T., Rowe, K. M., Leneman, D., Lai, H. R., et al. (2018). Insight auxiliary payload sensor suite (APSS). *Space Sci. Rev.* 215, 4. doi:10.1007/s11214-018-0570-x

Beamish, D., and Tzanis, A. (1986). High resolution spectral characteristics of the earth-ionosphere cavity resonances. *J. Atmos. Terr. Phys.* 48, 187–203. doi:10.1016/0021-9169(86)90084-x

Beghin, C. (2014). The atypical generation mechanism of Titan's Schumann resonance. *J. Geophys Res. Planets* 119, 520–531. doi:10.1002/2013JE004569

Brain, D., Halekas, J. S., Peticolas, L. M., Lin, R. P., Luhmann, J. G., Mitchell, D. L., et al. (2006). On the origin of aurorae on Mars. *Geophys. Res. Lett.* 33, 1–4. doi:10.1029/2005gl024782

Charalambous, C., McClean, J. B., Baker, M., Pike, W. T., Golombek, M., Lemmon, M., et al. (2021). Vortex-dominated aeolian activity at InSight's landing site, Part 1: multi-instrument observations, analysis, and implications. *JGR Planets* 126, e2020JE006757. doi:10.1029/2020JE006757

Cloutier, P. A., Law, C. C., Crider, D. H., Walker, P. W., Chen, Y., Acuña, M. H., et al. (1999). Venus-like interaction of the solar wind with Mars. *Geophys. Res. Lett.* 26, 2685–2688. doi:10.1029/1999gl900591

Connerney, J., Espley, J., Lawton, P., Murphy, S., Odom, J., Oliversen, R., et al. (2015). The MAVEN magnetic field investigation. *Space Sci. Rev.* 194, 257–291. doi:10.1007/s11214-015-0169-4

Duru, F., Baker, N., De Boer, M., Chamberlain, A., Verchimak, R., Morgan, D. D., et al. (2020). Martian ionopause boundary: coincidence with photoelectron boundary and response to internal and external drivers. *J. Geophys. Res. Space Phys.* 125, 27409. doi:10.1029/2019ja027409

Duru, F., Gurnett, D. A., Frahm, R. A., Winningham, J. D., Morgan, D. D., and Howes, G. G. (2009). Steep, transient density gradients in the Martian ionosphere similar to the ionopause at venus. *J. Geophys. Res. Space Phys.* 114, 4711. doi:10.1029/2009ja014711

Eden, H., and Vonnegut, B. (1973). Electrical breakdown caused by dust motion in low-pressure atmospheres: considerations for mars. *Science* 180, 962–963. doi:10.1126/science.180.4089.962

Esman, T. (2022). Magnetic field fluctuations from the solar wind to the surface of mars. Ph.D. thesis. Arizona: University of Arizona.

Esman, T. M., Espley, J., Gruesbeck, J., Fowler, C. M., Xu, S., Elrod, M., et al. (2022). Martian ionospheric magnetic fluctuations below 200 km. *JGR Space Phys.* 127, 30470. doi:10.1029/2022JA030470

Esman, T. M., Espley, J., Gruesbeck, J., Klein, K. G., and Giacalone, J. (2021). Plasma waves in the distant martian environment: implications for mars' sphere of influence. *J. Geophys. Res. Space Phys.* 126. doi:10.1029/2021ja029686

Farrell, W. M., and Desch, M. D. (2001). Is there a Martian atmospheric electric circuit? *J. Geophys. Res.* 106, 7591–7595. doi:10.1029/2000je001271

Farrell, W. M., Desch, M., Kaiser, M., Houser, J., Landis, G., and Wilt, D. (2000). Radio and optical detection of Martian dust storm discharges. *Acta Astronaut.* 46, 25–36. doi:10.1016/s0094-5765(99)00182-4

Farrell, W. M., Kaiser, M. L., Desch, M. D., Houser, J. G., Cummer, S. A., Wilt, D. M., et al. (1999). Detecting electrical activity from martian dust storms. *J. Geophys. Res.* 104 (3), 3795–3801. doi:10.1029/98je02821

Fowler, C., Andersson, L., Ergun, R. E., Morooka, M., Delory, G., Andrews, D. J., et al. (2015). The first *in situ* electron temperature and density measurements of the martian nightside ionosphere. *Geophys. Res. Lett.* 42, 8854–8861. doi:10.1002/2015GL065267

Füllekrug, M. (1995). Schumann resonances in magnetic field components. *J. Atmos. Terr. Phys.* 57, 479–484. doi:10.1016/0021-9169(94)00075-y

Girazian, Z., Halekas, J., and Lillis, R. J. (2023). Solar cycle and seasonal variability of the nightside ionosphere of mars: insights from five years of MAVEN observations. *Icarus* 393, 114615. doi:10.1016/j.icarus.2021.114615

Girazian, Z., Luppen, Z., Morgan, D. D., Chu, F., Montabone, L., Thiemann, E. M. B., et al. (2019). Variations in the ionospheric peak altitude at mars in response to dust storms: 13 years of observations from the mars express radar sounder. *JGR Planets* 125, 6092. doi:10.1029/2019je006092

Greifinger, C., and Greifinger, P. (1976). Transient ULF electric and magnetic fields following a lightning discharge. *J. Geophys. Res.* 81, 2237–2247. doi:10.1029/ja081i013p02237

Grimm, R. E. (2002). Low-frequency electromagnetic exploration for groundwater on Mars. *J. Geophys. Res. Planets* 107, 5006–5011. doi:10.1029/2001je001504

Gurnett, D. A., Huff, R., Morgan, D., Persoon, A., Averkamp, T., Kirchner, D., et al. (2008). An overview of radar soundings of the Martian ionosphere from the Mars Express spacecraft. *Adv. Space Res.* 41, 1335–1346. doi:10.1016/j.asr.2007.01.062

Gurnett, D. A., Morgan, D. D., Granroth, L. J., Cantor, B. A., Farrell, W. M., and Espley, J. R. (2010). Non-detection of impulsive radio signals from lightning in martian dust storms using the radar receiver on the mars express spacecraft: NO lightning from martian dust storms. *Geophys. Res. Lett.* 37, 44368. doi:10.1029/2010gl044368

Gurnett, D., Kirchner, D. L., Huff, R. L., Morgan, D. D., Persoon, A. M., Averkamp, T. F., et al. (2005). Radar soundings of the ionosphere of Mars. *Science* 310, 1929–1933. doi:10.1126/science.1121868

Guzewich, S. D., Lemmon, M., Smith, C. L., Martínez, G., de Vicente-Retortillo, Á., Newman, C. E., et al. (2019). Mars science laboratory observations of the 2018/Mars year 34 global dust storm. *Geophys. Res. Lett.* 46, 71–79. doi:10.1029/2018gl080839

Hansell, S. A., Wells, W., and Hunten, D. (1995). Optical detection of lightning on Venus. *Icarus* 117, 345–351. doi:10.1006/icar.1995.1160

Hanson, W. B., Sanatani, S., and Zuccaro, D. R. (1977). The Martian ionosphere as observed by the Viking retarding potential analyzers. *J. Geophys. Res.* 82, 4351–4363. doi:10.1029/js082i028p04351

Harper, J. M., Dufek, J., and McDonald, G. D. (2021). Detection of spark discharges in an agitated Mars dust simulant isolated from foreign surfaces. *Icarus* 357, 114268. doi:10.1016/j.icarus.2020.114268

Harter, B. (2022). Maven ancillary guidance navigation and control drf data collection. *NASA Planet. Data Syst.* doi:10.17189/15176721

Hauck, F. H. (2002). *Safe on Mars: Precursor measurements necessary to support human operations on the Martian surface*. Washington, DC: The National Academies Press.

Heavens, N. G., Johnson, M. S., Abdou, W. A., Kass, D. M., Kleinböhl, A., McCleese, D. J., et al. (2014). Seasonal and diurnal variability of detached dust layers in the tropical Martian atmosphere. *J. Geophys. Res.* 119, 1748–1774. doi:10.1002/2014je004619

Holzworth, R. H., McCarthy, M. P., Brundell, J. B., Jacobson, A. R., and Rodger, C. J. (2019). Global distribution of superbolts. *JGR Atmos.* 124, 9996–10005. doi:10.1029/2019JD030975

Houser, J. G., Farrell, W. M., and Metzger, S. M. (2003). ULF and ELF magnetic activity from a terrestrial dust devil. *Geophys. Res. Lett.* 30, 14144. doi:10.1029/2001GL014144

Izvekova, Y. N., Popel, S., and Izvekov, O. (2022). Dust and dusty plasma effects in schumann resonances on mars: comparison with earth. *Icarus* 371, 114717. doi:10.1016/j.icarus.2021.114717

Jakosky, B., Lin, R. P., Grebowsky, J. M., Luhmann, J. G., Mitchell, D. F., Beutelschies, G., et al. (2015). The mars atmosphere and volatile evolution (MAVEN) mission. *Space Sci. Rev.* 195, 3–48. doi:10.1007/s11214-015-0139-x

Joy, S., and Rowe, K. (2019). *InSight IFG data calibration description*. Planetary Data System.

Kim, E., Seo, H., Kim, J. H., Lee, J. H., Kim, Y. H., Choi, G. H., et al. (2012). The analysis of the topside additional layer of Martian ionosphere using MARSIS/Mars Express data. *J. Astronomy Space Sci.* 29, 337–342. doi:10.5140/JASS.2012.29.4.337

Kopf, A. J., Gurnett, D. A., DiBraccio, G. A., Morgan, D. D., and Halekas, J. S. (2017). The transient topside layer and associated current sheet in the ionosphere of Mars. *J. Geophys. Res. Space Phys.* 122, 5579–5590. doi:10.1002/2016JA023591

Kopf, A. J., Gurnett, D. A., Morgan, D. D., and Kirchner, D. L. (2008). Transient layers in the topside ionosphere of Mars. *Geophys. Res. Lett.* 35, L17102. doi:10.1029/2008GL034948

Krasnopolsky, V. A. (2006). A sensitive search for nitric oxide in the lower atmospheres of venus and mars: detection on venus and upper limit for mars. *Icarus* 182, 80–91. doi:10.1016/j.icarus.2005.12.003

Krauss, C. E., Horányi, M., and Robertson, S. (2006). Modeling the formation of electrostatic discharges on Mars. *J. Geophys. Res.* 111, 2313. doi:10.1029/2004je002313

Ksanfomaliti, L. V. (1980). Discovery of frequent lightning discharges in clouds on Venus. *Nature* 284, 244–246. doi:10.1038/284244a0

Kurth, W. S., Hospodarsky, G. B., Kirchner, D. L., Mokrzycki, B. T., Averkamp, T. F., Robison, W. T., et al. (2017). The juno waves investigation. *Space Sci. Rev.* 213, 347–392. doi:10.1007/s11214-017-0396-y

Lillis, R., Fillingim, M. O., Peticolas, L. M., Brain, D. A., Lin, R. P., and Bougher, S. W. (2009). Nightside ionosphere of mars: modeling the effects of crustal magnetic fields and electron pitch angle distributions on electron impact ionization. *J. Geophys. Res.* 114, E11009. doi:10.1029/2009je003379

Matta, M., Mendillo, M., Withers, P., and Morgan, D. (2015). Interpreting Mars ionospheric anomalies over crustal magnetic field regions using a 2-D ionospheric model. *J. Geophys. Res. Space Phys.* 120, 766–777. doi:10.1002/2014ja020721

Mayyasi, M., Withers, P., and Fallows, K. (2018). A sporadic topside layer in the ionosphere of Mars from analysis of MGS radio occultation data. *J. Geophys. Res. Space Phys.* 123, 883–900. doi:10.1002/2017JA024938

Melnik, O., and Parrot, M. (1998). Electrostatic discharge in martian dust storms. *J. Geophys. Res.* 103, 29107–29117. doi:10.1029/98ja01954

Mitchell, D. L., Lin, R. P., Mazelle, C., Rème, H., Cloutier, P. A., Connerney, J. E. P., et al. (2001). Probing Mars' crustal magnetic field and ionosphere with the MGS electron reflectometer. *J. Geophys. Res.* 106, 23419–23427. doi:10.1029/2000je001435

Molina-Cuberos, G. J., Morente, J. A., Besser, B. P., Portí, J., Lichtenegger, H., Schwingenschuh, K., et al. (2006). Schumann resonances as a tool to study the lower ionospheric structure of Mars. *Radio Sci.* 41, 3187. doi:10.1029/2004rs003187

Montabone, L., Spiga, A., Kass, D. M., Kleinböhl, A., Forget, F., and Millour, E. (2020). Martian year 34 column dust climatology from mars climate sounder observations: reconstructed maps and model simulations. *JGR Planets* 125, e2019JE006111. doi:10.1029/2019JE006111

Němec, F., Morgan, D. D., Gurnett, D. A., and Brain, D. A. (2011). Areas of enhanced ionization in the deep nightside ionosphere of Mars. *J. Geophys. Res.* 116, E06006. doi:10.1029/2011je003804

Němec, F., Morgan, D. D., Gurnett, D. A., and Duru, F. (2010). Nightside ionosphere of mars: radar soundings by the mars express spacecraft. *J. Geophys. Res.* 115, E12009. doi:10.1029/2010je003663

Nickolaenko, A. P., and Hayakawa, M. (2002). *Modern approaches in geophysics*. Doredrecht/Boston/London: Kluwer Academic Publishers Resonances in the Earth-ionosphere Cavity.

Nielsen, E., Fraenz, M., Zou, H., Wang, J. S., Gurnett, D., Kirchner, D., et al. (2007). Local plasma processes and enhanced electron densities in the lower ionosphere in magnetic cusp regions on Mars. *Planet. Space Sci.* 55, 2164–2172. doi:10.1016/j.pss.2007.07.003

PDS (2007). Mars global surveyor premap mag data. *NASA Planet. Data Syst.* doi:10.17189/1519755

PDS (2022). Maven magnetometer (mag) calibrated data bundle. *NASA Planet. Data Syst.* doi:10.17189/1414178

Pechony, O., and Price, C. (2004). Schumann resonance parameters calculated with a partially uniform knee model on Earth, Venus, Mars, and Titan. *Radio Sci.* 39, 3056. doi:10.1029/2004rs003056

Renno, N. O., Wong, A. S., Atreya, S. K., de Pater, I., and Roos-Serote, M. (2003). Electrical discharges and broadband radio emission by martian dust devils and dust storms. *Geophys. Res. Lett.* 30, 1. doi:10.1029/2003gl017879

Riousset, J. A., Nag, A., and Palotai, C. (2020). Scaling of conventional breakdown threshold: impact for predictions of lightning and TLEs on earth, venus, and mars. *Icarus* 338, 113506. doi:10.1016/j.icarus.2019.113506

Ruf, C., Renno, N. O., Kok, J. F., Bandelier, E., Sander, M. J., Gross, S., et al. (2009). Emission of non-thermal microwave radiation by a Martian dust storm. *Geophys. Res. Lett.* 36, L13202. doi:10.1029/2009gl038715

Russell, C. T., Clayton, R. N., Buseck, P. R., Hua, X., Holsapple, K. A., Esposito, L. W., et al. (1993). Planetary lightning. *Annu. Rev. Earth Planet. Sci.* 21, 43–87. doi:10.1146/annurev.ea.21.050193.000355

Russell, C. T. (1995). *Introduction to space Physics*. Cambridge, UK: Cambridge University Press.

Russell, C. T., and Joy, S. P. (2021). Insight IFG mars bundle. *NASA Planet. Data Syst.* doi:10.17189/1519207

Russell, C. T., Strangeway, R., and Zhang, T. (2006). Lightning detection on the venus express mission. *Planet Space Sci.* 54, 1344–1351. doi:10.1016/j.pss.2006.04.026

Russell, C. T. (1991). *Venus aeronomy*. Dordrecht/Boston/London: Kluwer Academic Publishers, 1–4. chap. Venus Lightning.

Safaeinili, A., Kofman, W., Mouginot, J., Gim, Y., Herique, A., Ivanov, A. B., et al. (2007). Estimation of the total electron content of the Martian ionosphere using radar sounder surface echoes. *Geophys. Res. Lett.* 34, L23204. doi:10.1029/2007GL032154

Schumann, U., and Huntrieser, H. (2007). The global lightning-induced nitrogen oxides source. *Atmos. Chem. Phys.* 7, 3823–3907. doi:10.5194/acp-7-3823-2007

Schumann, W. O. (1952). Über die strahlungslosen Eigenschwingungen einer leitenden Kugel, die von einer Luftschicht und einer Ionosphärenhülle umgeben ist. *Z. Naturforsch. Teil A* 7, 149–154. doi:10.1515/zna-1952-0202

Sentman, D. D., and Fraser, B. J. (1991). Simultaneous observations of schumann resonances in California and Australia - evidence for intensity modulation by the local height of the d region. *J. Geophys. Res.* 96, 15973–15984. doi:10.1029/91JA01085

Sentman, D. D. (1995). *Handbook of atmospheric electrodynamics*. Boca Raton/London/New York: CRC Press, Taylor and Francis Group.

Shirley, J. H. (2015). Solar system dynamics and global-scale dust storms on Mars. *Icarus* 251, 128–144. doi:10.1016/j.icarus.2014.09.038

Simoes, F., Grard, R., Hamelin, M., López-Moreno, J., Schwingenschuh, K., Béghin, C., et al. (2008a). The schumann resonance: A tool for exploring the atmospheric environment and the subsurface of the planets and their satellites. *Icarus* 194, 30–41. doi:10.1016/j.icarus.2007.09.020

Simoes, F., Pfaff, R., and Freudenreich, H. (2011). Satellite observations of Schumann resonances in the Earth's ionosphere. *Geophys. Res. Lett.* 38, 49668. doi:10.1029/2011GL049668

Simoes, F., Rycroft, M., Renno, N., Yair, Y., Aplin, K. L., and Takahashi, Y. (2008b). Schumann resonances as a means of investigating the electromagnetic environment in the solar system. *Space Sci. Rev.* 137, 455–471. doi:10.1007/s11214-008-9398-0

Soriano, A., Navarro, E. A., Morente, J. A., and Portí, J. A. (2007). A numerical study of the Schumann resonances in Mars with the FDTD method. *J. Geophys. Res.* 112, A06311. doi:10.1029/2007JA012281

Sukhorukov, A. I. (1991). On the schumann resonances on mars. *Planet. Space Sci.* 39, 1673–1676. doi:10.1016/0032-0633(91)90028-9

Toledo-Redondo, S., Salinas, A., Portí, J., Witasse, O., Cardnell, S., Fornieles, J., et al. (2017). Schumann resonances at mars: effects of the day-night asymmetry and the dust-loaded ionosphere. *GRL* 44, 648–656. doi:10.1002/2016GL071635

Torrence, C., and Compo, G. P. (1998). A practical guide to wavelet analysis. *Bull. Am. Meteorological Soc.* 79, 61–78. doi:10.1175/1520-0477(1998)079<0061:apgtwa>2.0.co;2

Turman, B. N. (1977). Detection of lightning superbolts. *JGR* 82, 2566–2568. doi:10.1029/JC082i018p02566

Vogt, M. F., Withers, P., Fallows, K., Andersson, L., Girazian, Z., Mahaffy, P. R., et al. (2016). MAVEN observations of dayside peak electron densities in the ionosphere of Mars. *J. Geophys. Res. Space Phys.* 122, 891–906. doi:10.1002/2016ja023473

Votis, C. I., Tatsis, G., Christofilakis, V., Chronopoulos, S. K., Kostarakis, P., Tritakis, V., et al. (2018). A new portable elf schumann resonance receiver: design and detailed analysis of the antenna and the analog front-end. *J. Wirel. Com. Netw.* 155, 155. doi:10.1186/s13638-018-1157-7

Withers, P., Felici, M., Mendillo, M., Moore, L., Narvaez, C., Vogt, M. F., et al. (2018). First ionospheric results from the MAVEN radio occultation science experiment (ROSE). *J. Geophys. Res. Space Phys.* 123, 4171–4180. doi:10.1029/2018ja025182

Withers, P., Fillingim, M. O., Lillis, R. J., Häusler, B., Hinson, D. P., Tyler, G. L., et al. (2012). Observations of the nightside ionosphere of mars by the mars express radio science experiment (MaRS). *J. Geophys. Res.* 117, 18185. doi:10.1029/2012ja018185

Withers, P., Mendillo, M., and Hinson, D. P. (2006). Space weather effects on the Mars ionosphere due to solar flares and meteors. *Eur. Planet. Sci. Congr.* 190, 2.

Yair, Y. (2012). New results on planetary lightning. *Adv. Space Res.* 50, 293–310. doi:10.1016/j.asr.2012.04.013

Yang, H., Pasko, V. P., and Yair, Y. (2006). Three-dimensional finite difference time domain modeling of the Schumann resonance parameters on Titan, Venus, and Mars. *Radio Sci.* 41, 3431. doi:10.1029/2005RS003431

Zhai, Y., Cummer, S. A., and Farrell, W. M. (2006). Quasi-electrostatic field analysis and simulation of martian and terrestrial dust devils. *J. Geophys. Res.* 111, E06016. doi:10.1029/2005JE002618

Zhang, Z., Orosei, R., Huang, Q., and Zhang, J. (2015). Topside of the martian ionosphere near the terminator: variations with season and solar zenith angle and implications for the origin of the transient layers. *Icarus* 251, 12–25. doi:10.1016/j.icarus.2014.09.036